ACS Infectious Diseases

pubs.acs.org/journal/aidcbc

Article

Contact Dynamics of Cytoadhering *Plasmodium falciparum*-Infected Erythrocytes in Flow

Katharina Scholz, Marianne Papagrigorakes, Leon Lettermann, Federica Pennarola, Pintu Patra, Anil Kumar Dasanna, Cecilia P. Sanchez, Jessica Kehrer, Elisabetta Ada Cavalcanti-Adam, Ulrich S. Schwarz,* Motomu Tanaka,* and Michael Lanzer*

Cite This: https://doi.org/10.1021/acsinfecdis.5c00594

Read Online

ACCESS | Metrics & More | Article Recommendations | Supporting Information

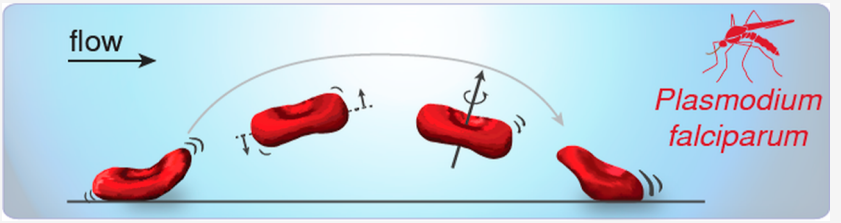

ABSTRACT: The virulence of the human malaria parasite *Plasmodium falciparum* is linked to the altered mechanical and adhesive properties of infected erythrocytes, which adhere to the microvascular endothelium to evade splenic clearance. The underlying biophysical mechanisms remain incompletely understood, particularly regarding the contact area and bond landscape, due in part to the rapid and transient nature of these interactions. In this study, we investigated the dynamic adhesion behavior of *P. falciparum*-infected erythrocytes on surfaces functionalized with intercellular adhesion molecule 1 (ICAM-1), cluster of differentiation 36 (CD36), or a combination of both. To this end, we employed DNA-based molecular force sensors, high-speed reflection interference contrast microscopy, and computer simulations. Our results show that trophozoite-stage infected erythrocytes, which maintain a discoidal shape, exhibit complex motion behaviors across all substrates, including flipping over the long axis and flipping combined with lateral sliding, with or without pinning, producing patchy adhesion footprints. In contrast, schizont-stage parasites display a more uniform rolling motion, occasionally accompanied by sliding or pinning, consistent with their spherical morphology and stiffened membrane. We further observed that the incidence of sliding increased on CD36-containing surfaces for both developmental stages. Notably, some adhesion footprints extended across distances comparable to the length of an endothelial cell. Together, these findings provide new insights into the complex biophysical adaptations of *P. falciparum*-infected erythrocytes, offering a more detailed understanding of the mechanisms driving cytoadhesion and its potential impact on microvasculature pathology.

KEYWORDS: *malaria, adhesion dynamics, molecular force sensor, reflection interference microscopy, supported membrane*

Malaria claims a life every 50 s, with most deaths attributed to the protozoan parasite *Plasmodium falciparum*.[1] Transmitted by Anopheles mosquitos, the parasite first infects hepatocytes before shifting to erythrocytes, establishing a 48 h intra-erythrocytic life cycle during which the parasites develop from ring stages to trophozoites and then to schizonts before the release of daughter cells. The intraerythrocytic life cycle causes a broad range of symptoms ranging from fevers to gastrointestinal malaise to multiorgan failure. These life-threatening complications arise from altered biophysical properties of infected erythrocytes and their ability to sequester in the microvasculature via acquired cytoadhesive traits.[2]

To thrive within erythrocytes, the parasite remodels them.[3] For example, it repurposes the actin from the erythrocyte membrane skeleton and generates long actin filaments required for vesicular transport of parasite-encoded proteins to the surface.[4−6] As a result, the infected erythrocyte loses its discoidal shape and begins to roundup, a process furthered by the influx of Na^+ and accompanying water via parasite-induced new permeation pathways.[7] Additionally, the parasite catabolizes large amounts of hemoglobin for dietary purposes and to maintain the osmo-colloidal balance of the infected cell in light of its space-demanding anabolic activities.[8] The parasite further establishes de novo supramolecular structures underneath the erythrocyte plasma membrane, termed knobs.[9−11] Knobs connect actin-deprived spectrin filaments and serve as platforms

Received: July 19, 2025
Revised: July 28, 2025
Accepted: July 30, 2025

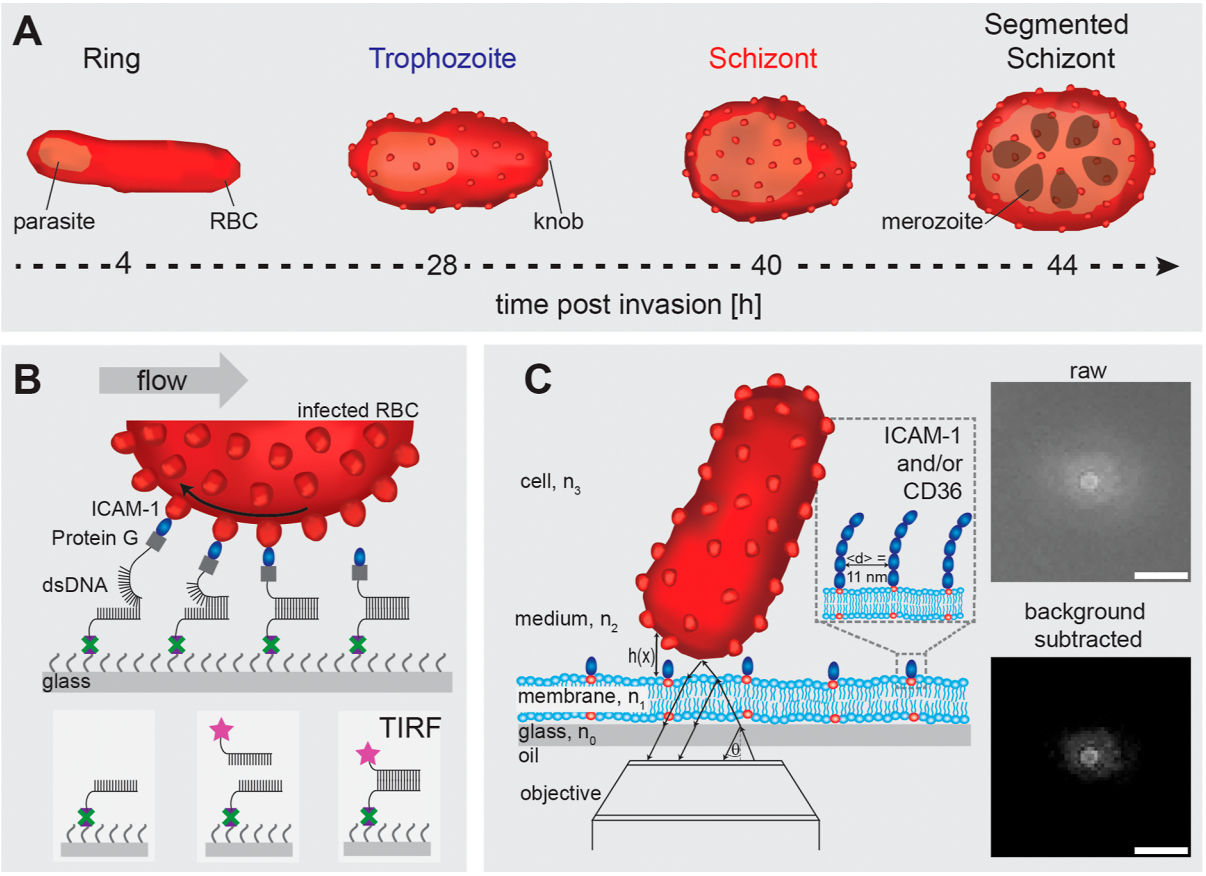

Figure 1. Experimental strategy. (A) Schematic representation of the intraerythrocytic developmental stages of *P. falciparum*. (B) Schematic illustrating the adhesion force sensor assay. Infected erythrocytes bind to ICAM-1 via PfEMP1, with ICAM-1 attached to the Watson strand of a DNA duplex. The Crick strand of the duplex is firmly conjugated to the glass surface. Disrupted DNA duplexes are visualized using a fluorescently labeled DNA probe complementary to the Crick strand, and the resulting footprint is observed using total internal reflection fluorescence (TIRF) microscopy. (C) Infected erythrocytes interact with supported membranes functionalized with ICAM-1, CD36, or both. Interference from monochromatic light reflections is recorded, with image brightness primarily reflecting light scattered by the digestive vacuole and inversely correlating with its distance to the surface. Phases: n_1–n_3. Image rate: 250 fps (4 ms/frame). Average receptor spacing: ⟨d⟩ = 11 nm. Scale bar: 5 μm.

for the presentation of adhesins, anchoring them to the membrane skeleton.[9,12,13] As a result of these alterations, the erythrocyte plasma membrane stiffens.[6,14−17] Parasite lines lacking knobs do not cytoadhere under flow and are removed from circulation by the spleen.[18]

P. falciparum encodes several classes of immune-variant adhesins, of which the PfEMP1 family is the most prominent and best studied, enabling adhesive interactions with receptors present on endothelial cells, platelets, or in the placental intervillous space, such as intercellular adhesion molecule 1 (ICAM-1), cluster of differentiation 36 (CD36), endothelial protein C receptor, or chondroitin-4-sulfate.[19,20] While the molecular players and the pathology of cytoadhesion are increasingly understood, the temporal and spatial aspects of contact dynamics under flow remain poorly understood, in spite of the fact that contact dynamics influences how long infected erythrocytes persist in the vasculature and to what extent the endothelium is activated.[21,22] Endothelial cell activation promotes cytoadhesion and vaso-occlusion by upregulating and clustering adhesion receptors.[23−25]

To probe the biophysical mechanisms and consequences of these adhesive interactions, a range of experimental approaches have been employed. For instance, adhesion forces were measured using atomic force microscopy by bringing infected erythrocytes into contact with CHO cells, endothelial monolayers, or defined adhesion receptors such as CD36 and ICAM-1.[23,26−29] In comparison, microfluidic flow chamber experiments, using various surface models including (i) direct immobilization of receptors,[20,29−31] (ii) endothelial monolayers,[22−24,32−35] and (iii) supported lipid bilayers[36−38], dissected individual receptor contributions, assessed endothelial activation and adhesion receptor presentation, and allowed control over receptor density and mechanical stability of adhesion under flow.

During dynamic adhesion events—such as those involving infected erythrocytes or leukocytes—receptor−ligand bonds form and dissociate within milliseconds, with only a small fraction of available receptors and ligands participating at any given time.[13,32,33,39−42] The spatial and temporal characteristics of these interactions, often referred to as the "bond landscape", are difficult to resolve using conventional assays. To address this gap, we employed a molecular adhesion footprint assay, high-speed reflection interference contrast microscopy (HS-RICM), and computer simulations to visualize and quantify the adhesion dynamics of infected erythrocytes under flow with a high spatial and temporal resolution.

RESULTS

Experimental Approaches. Figure 1 illustrates the strategies we used to investigate the dynamic adhesion behavior

https://doi.org/10.1021/acsinfecdis.5c00594
ACS Infect. Dis. XXXX, XXX, XXX−XXX

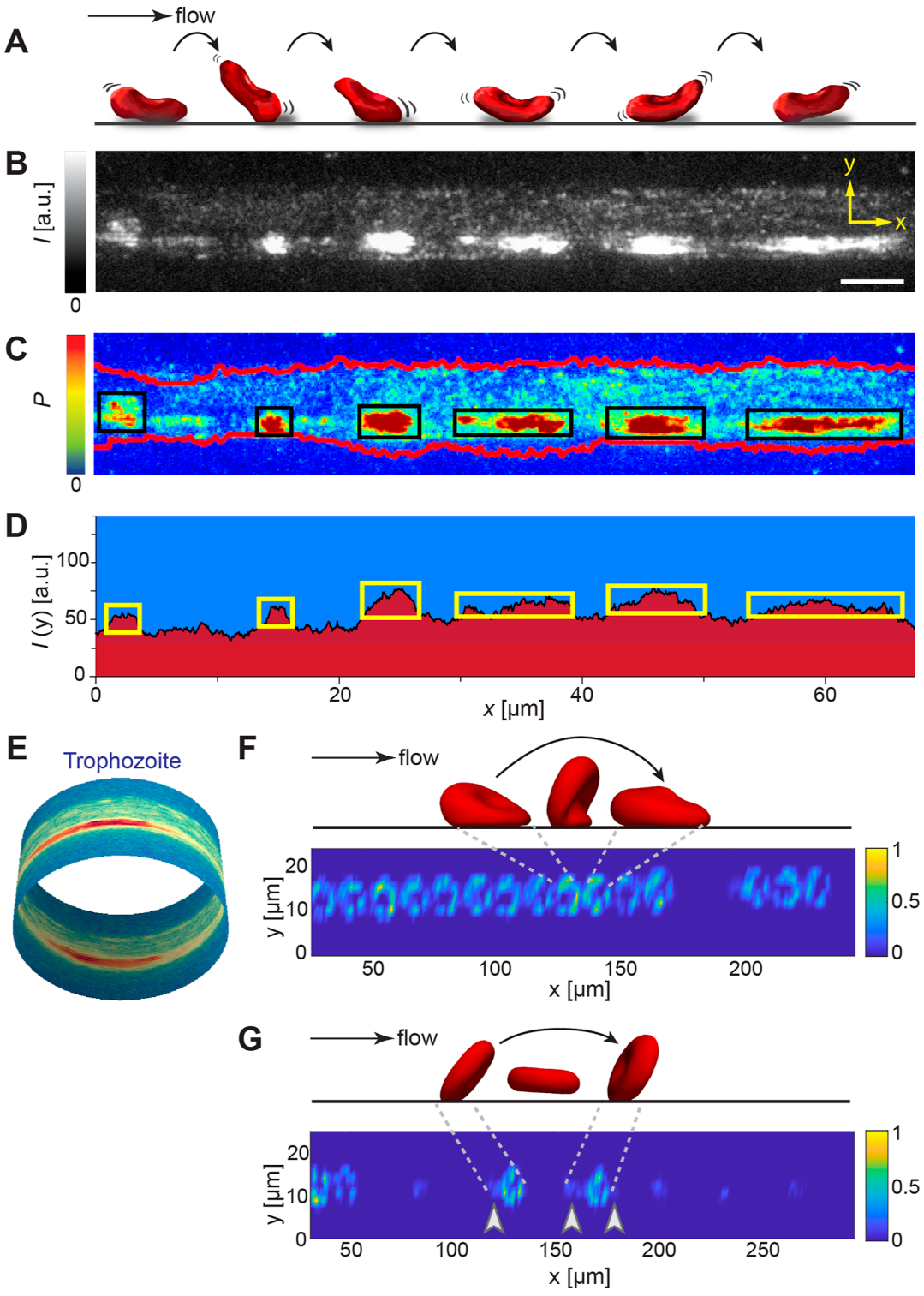

Figure 2. Footprint of a flipping trophozoite visualized by the adhesion force sensor assay. (A) Schematic of a flipping trophozoite. (B) Representative TIRF image showing a patchy fluorescence footprint; grayscale reflects contact density. Shear stress: 0.1 Pa. Scale bar: 5 μm. (C) Contact probability (P) along the x-axis, color-coded from blue (0) to red (100); black boxes highlight high-probability patches. Red lines delineate the upper and lower borders of the footprint. (D) Average fluorescence intensity (I) along the x-axis. (E) 3D projection of the footprint on a 7.2 μm diameter cylinder, showing high probability adhesion zones (red) opposite each other; rim profile circumference: 22 μm. (F) Top: simulated snapshots of a flipping trophozoite. Shear stress of ≃0.11 Pa. Bottom: corresponding contact map (note elongated y-axis scaling). (G) Simulated irregular flipping under 0.14 Pa, with footprint below; greater spacing between contact patches indicates intermittent detachment. Arrowheads mark sliding-like contacts. For both cases, on/off rates = 0.5$\dot{\gamma}$.

of *P. falciparum*-infected erythrocytes under flow. As surrogate endothelial cell surfaces, we employed reconstructed substrates containing different adhesion receptors, including ICAM-1, CD36, and a combination of both. To account for the different intraerythrocytic parasite stages and their different shapes, biomechanical properties, and cytoadhesiveness, we focused on

https://doi.org/10.1021/acsinfecdis.5c00594
ACS Infect. Dis. XXXX, XXX, XXX−XXX

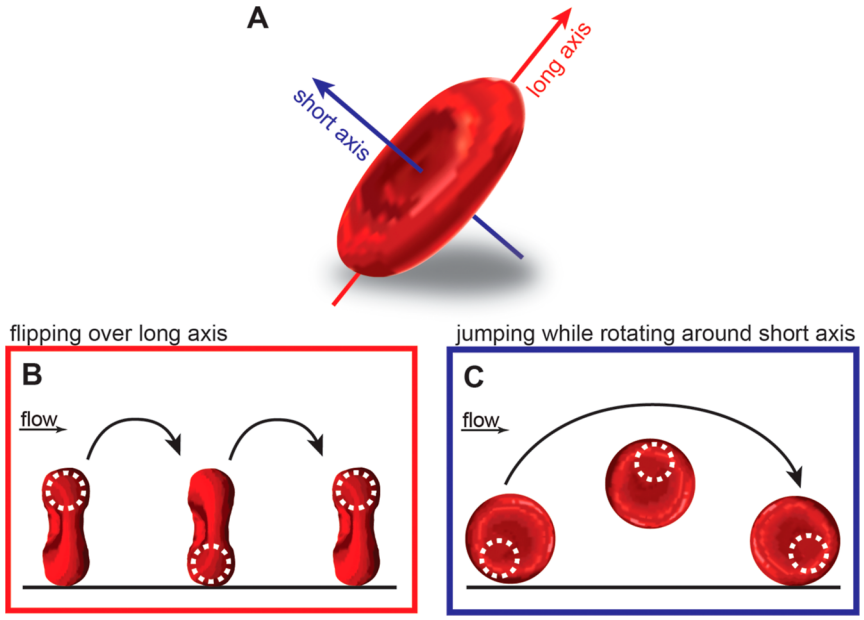

Figure 3. Schematic of erythrocyte geometry and rotation modes. (A) Cartoon of an erythrocyte showing its "long axis" and "short axis". (B) Flipping motion around the long axis ("coin-like"). (C) Rotational motion around the short axis ("wheel-like").

two key stages: trophozoites (24−30 h post invasion) and schizonts (36 to 42 h post invasion) (Figure 1A). Trophozoites retain a biconcave shape and a flexible membrane, whereas schizonts are spherical and rigid, with the cytoadhesive potential increasing as the parasite develops.[7,14,15,22]

The first strategy involves a molecular force sensor assay based on DNA tension gauge tethers (TGTs), originally developed to study rolling adhesion of leukocytes and cancer cells.[43] In this assay, adhesion receptors are coupled to a hybridized double-stranded DNA (dsDNA) tether immobilized on the substrate (Figure 1B). As the cell moves over the surface, receptor−ligand bonds are formed, and the DNA duplexes are opened due to physical forces at the cell−substrate interface, leaving single stranded DNA oligomers behind as indicators of productive contact points. The contact points are then visualized using a fluorescently labeled complementary DNA probe, revealing the molecular adhesion footprint of the cell/surface interaction over a certain period and under defined flow conditions. Imaging is performed using TIRF microscopy (Figure 1B).

As a second strategy, we applied HS-RICM (Figure 1C). HS-RICM detects nanometer-scale variations in cell−surface proximity based on the interference of light reflected between compartments with different refractive indices.[44] This technique provides high temporal (250 frames per second) and spatial resolution, allowing us to track dynamic adhesion events during cell movement under a defined shear stress. The third approach involved computer simulations using a deformable red blood cell model and multiparticle collision hydrodynamics.[22]

Contact Landscapes Indicate Flipping of Trophozoites and Rolling of Schizonts. For the adhesion footprint assay, an 18-base pair DNA duplex was used with the Watson strand coupled to an Fc-ICAM-1 chimera and the Crick strand immobilized on biotin-PEG-coating via neutravidin bridges (Figure 1B). The amount of DNA duplexes was adjusted to yield a density of ∼400 ICAM-1 molecules per μm^2. Each step in the production process was controlled and verified (Figure S1). Since unzipping the DNA duplex entails a productive receptor−ligand interaction, the assay is highly sensitive and capable of detecting single bonds. The force required to unzip an 18mer DNA duplex depends on the loading conditions, but it is generally estimated to exceed $F^* \approx 12$ pN.[43,45,46] Since the fluorescence signal intensity is proportional to the number of ruptured DNA duplexes, at least at similar loading conditions as expected for our low-hematocrit assays, regions of high signal intensity indicate areas with a high density of adhesion contact points.

Figures 2A−D depict the footprint of a *P. falciparum*-infected erythrocyte at the trophozoite stage. The corresponding FCR3 line was preselected for cytoadhesion to ICAM-1 prior to the assay. The footprint displays a recurring patchy pattern characterized by regions of high fluorescence intensity interspersed within a broader band of diffuse, low-density signals. Analysis of 21 tracks revealed that most of the adhesion footprints exhibited a periodic arrangement (Figure S2), whereas uninfected erythrocytes did not leave any traces when examined in parallel, confirming the specificity of the experimental setup (Figure S1).

Parameterization of the tracks using a customized script yielded quantitative average measurements (±SD) for several parameters: the footprint width (6.0 ± 1.8 μm) and length (58.0 ± 16.7 μm); the center-to-center distance between patches (18.3 ± 7.6 μm; n = 80 patches from 14 tracks); the area of the patches (4.4 ± 7.7 μm^2; n = 80 patches); the length of the patches (1.6 ± 0.6 μm; n = 80 patches); and the overall surface density profile of the disruption force (Figures 2C,D and S3). Projecting these parameters onto a cylindrical body with geometric features of an erythrocyte (a radius of 3.6 μm and a circumference of 22.6 μm)[47] revealed that the interaction with the substrate primarily occurs at two opposing zones (Figure 2E), in spite of the fact that the erythrocyte surface is covered with thousands of knobs, each presenting 3 to 4 PfEMP1 molecules.[48] This contact landscape suggests a flipping motion, with trophozoites flipping over their long axis (i.e., face-overface) rather than rolling and jumping around their short axis (rolling along the rim) (Figure 3). Additionally, based on the footprint width (∼6.0 μm), the cell's broad surface seems to

https://doi.org/10.1021/acsinfecdis.5c00594
ACS Infect. Dis. XXXX, XXX, XXX−XXX

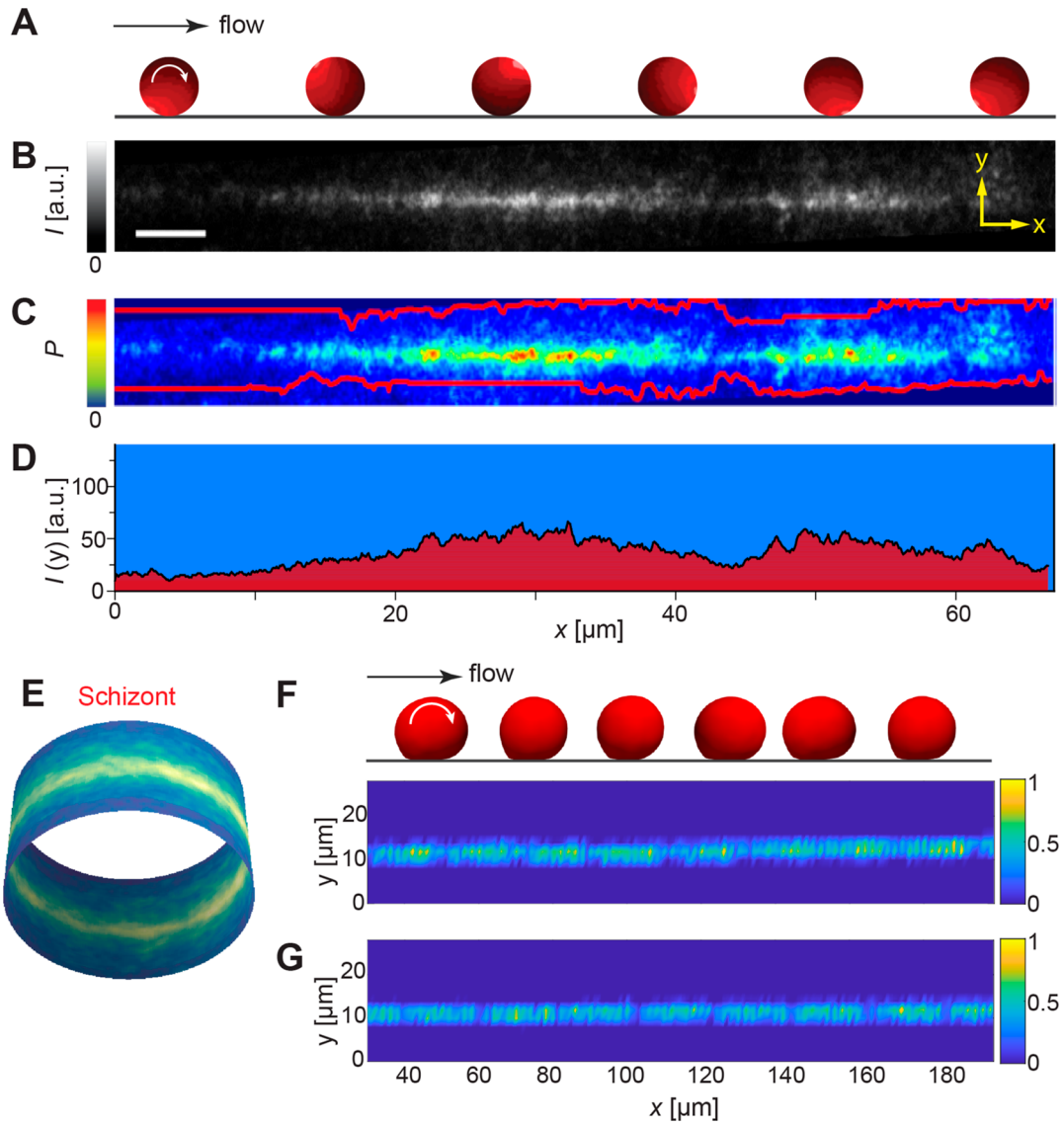

Figure 4. Footprint of a schizont revealed by adhesion force sensor assay. (A) Schematic of a rolling schizont. (B) Representative TIRF image showing a uniform fluorescence footprint, indicating continuous contact. Grayscale intensity corresponding to fluorescence intensity. Shear stress: 0.1 Pa. Scale bar: 5 μm. (C) Contact probability (P) along the x-axis, with red lines marking footprint boundaries and black boxes highlighting high-contact regions. (D) Average fluorescence intensity (I) across the x-axis. (E) 3D cylindrical projection (7.2 μm diameter) of the schizont path showing continuous contact around the circumference. (F,G) Simulation snapshots and corresponding contact footprints at low (≃0.085 Pa) and high (≃0.114 Pa) shear stress. Knob density for schizonts was set 1.6× higher than for trophozoites.[72]

engage with and disengage from the substrate, likely due to the wall shear stress pressing the cell against the surface once its free movement in flow is constrained by productive adhesion.

To gain additional insights into the motion of trophozoites, we simulated the adhesion footprint by integrating the semidiscoidal geometry and cellular mechanics of a trophozoite, the overall random distribution of knobs-anchored adhesins over the surface, a deformable red blood cell model, and hydrodynamic flow simulated by multiparticle collision dynamics.[22,49,50] Bonds were assumed to form with a constant rate given spatial proximity and to break as slip bonds, which means that they break faster at higher forces and dependent on loading rate.[51] Additionally, we assessed the impact of shear stress on the adhesion dynamics. The simulation revealed that at low shear stress, the footprint is highly periodic, revealing evenly spaced face-to-surface contacts, characteristic of a pure flipping motion (Figure 2F). In contrast, at higher shear stress, the footprint became less regular, with fewer high-density contact patches, variable patch sizes, and inconsistent spacing between patches (Figure 2G). Some patches also exhibited lateral extensions in both directions (Figure 2G), suggestive of pre- and postattachment interactions with the substrate, potentially due to slipping or crawling over the substrate. Notably, the simulated cells were also flipping over their long axis, consistent with the experimental data. In comparison, the experimental track widths (in the y direction) could not be reproduced by the simulations and remained largely unaffected by shear rate, suggesting that infected erythrocytes have deformation modes not represented in the simulations. In summary, trophozoite adhesion is predominantly governed by flipping, while wall stress modulates both the spacing and length of high-density contact zones, the latter likely due to slipping or crawling.

We next investigated the schizonts. Their footprints were narrow (1.6 ± 1.7 μm in width, $n = 21$), continuous and uniform

https://doi.org/10.1021/acsinfecdis.5c00594
ACS Infect. Dis. XXXX, XXX, XXX−XXX

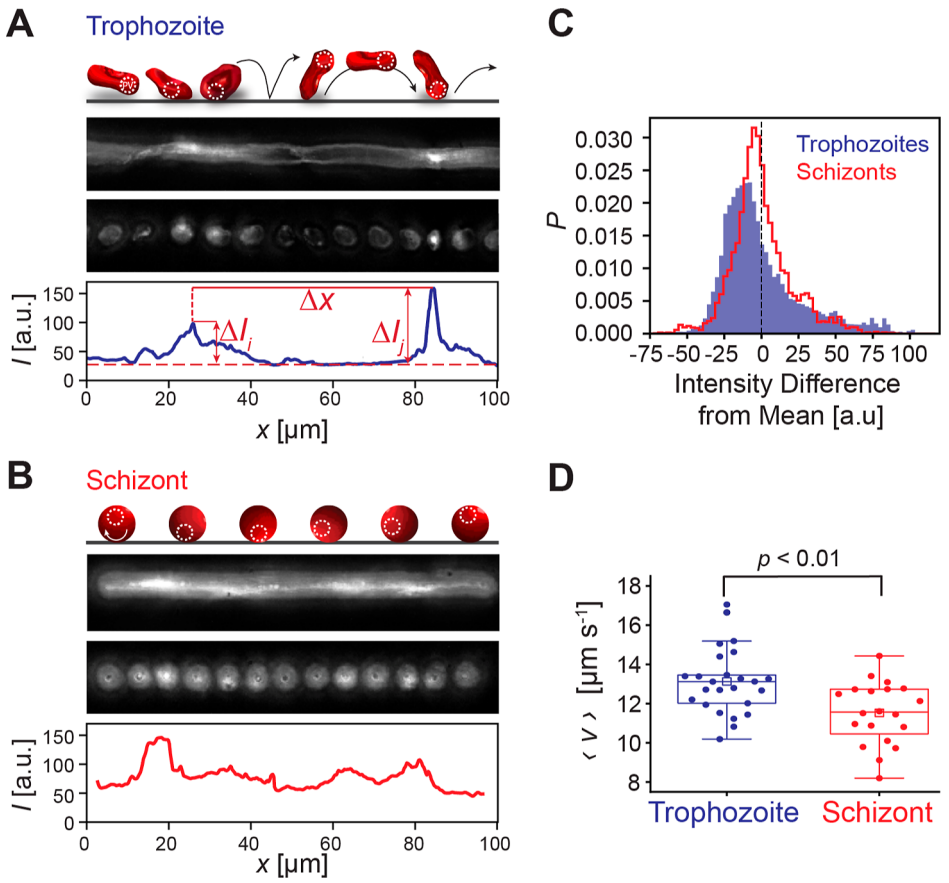

Figure 5. Spatial patters of dynamic adhesion captured by HS-RICM. (A) Trophozoite-stage cell. Top to bottom—schematic of flipping motion, maximum intensity projection, time-lapse snapshots (Δt = 0.6 s), and integrated signal intensity (I) as a function of distance (x). Periodic peaks in intensity (Δx = 57.1 ± 14.8 μm) reflect full rotations (360°) as the digestive vacuole nears the surface. See Figure S5 for full sequence. (B) Schizont-stage cell (see also Figure S5). (C) Probability density of intensity differences (ΔI) reveals asymmetric distribution for trophozoites vs symmetric, homogeneous profiles for schizonts (D) Mean translational velocity $\langle v \rangle$ for trophozoites (N = 25) and schizonts (N = 21). Each point represents an independent determination (box plot analysis, see Materials and Methods). Statistical analysis according to Student's t-test.

and had a length of 44.6 ± 12.8 μm (Figures 4A–D, S2 and S3). Such a contact pattern aligns with a hard, spherical body rolling over a surface along its circumference, as indicated by a 3D projection of the footprint and simulations considering the size, shape, and membrane properties of infected erythrocytes at the schizont stage (Figure 4E–G). While the simulated tracks align well with the experimental footprints, the simulated tracks appear more continuous than the experimental data, with the contact areas decreasing with increasing shear rates (Figure 4F,G).

Real-Time Imaging of Adhesion Dynamics with HS-RICM. Figure 5A shows the HS-RICM maximum intensity projection and the time lapse frames (at 0.6 s for visual clarity) of a trophozoite-stage infected erythrocyte interacting with an ICAM-1-functionalized supported lipid bilayer under flow (mean intermolecular ICAM-1 distance $\langle d \rangle$ = 11 nm). Bright signals originate mainly from light scattering by the parasite digestive vacuole,[14] with signal intensity increasing as the digestive vacuole approaches the surface.

The maximum intensity projection revealed a pattern of intermittent bright segments alternating with low-intensity regions (Figure 5A), indicative of periodic cell–surface contacts. These high-intensity segments correspond to prolonged surface contacts caused by adhesive interactions that temporarily slow the cell's movement. This pattern is characteristic of a flipping motion over the long axis, which is further illustrated by time-lapse sequences (Figure 5A). The average peak-to-peak distance (Δx = 57.1 ± 14.8 μm, n = 25) reflects the distance traveled by the cell while rotating by 360°. It is notably greater than the cell's diameter (7–8 μm[47]), suggesting transient detachment during flipping, frequently accompanied by tumbling and twisting (Movie S1).

In contrast, schizont-stage infected erythrocytes displayed continuous bright tracks in maximum intensity projections and time-lapse sequences, indicating stable, prolonged contact consistent with rolling (Figure 5B, Movie S2). Accordingly, the deviation of the signal intensity from the mean ($\Delta I(t) = I(t) - \langle I(t) \rangle$) was narrower and more symmetric than that of the trophozoites (Figure 5C). Additionally, schizonts traveled slower ($\langle v_{\text{schizont}} \rangle \approx 11.3 \pm 2.5$ μm s^{-1}) than trophozoites ($\langle v_{\text{troph}} \rangle \approx 13.1 \pm 3.6$ μm s^{-1}, n = 25); n = 25; $p < 0.01$, Student's t-test (Figure 5D), likely due to friction-induced slowing of the rolling schizonts.

Relating the real-time intensity profiles to the velocity data offered additional quantitative insights into the differential adhesion dynamics of trophozoites and schizont. For a representative trophozoite, the time to complete a full rotation of 360° is given by the peak-to-peak interval (Δt_i = 4.7 s) (Figure 6A), while the mean periodicity of rotation was Δt = 4.4 ± 1.3 s (n = 25) (Figure 6C) and the average contact time was $\langle t_c \rangle$ = 1.3 ± 0.5 s (Figure 6D). The latter was determined from full width at half-maximum of the intensity peaks after subtraction of the

https://doi.org/10.1021/acsinfecdis.5c00594
ACS Infect. Dis. XXXX, XXX, XXX–XXX

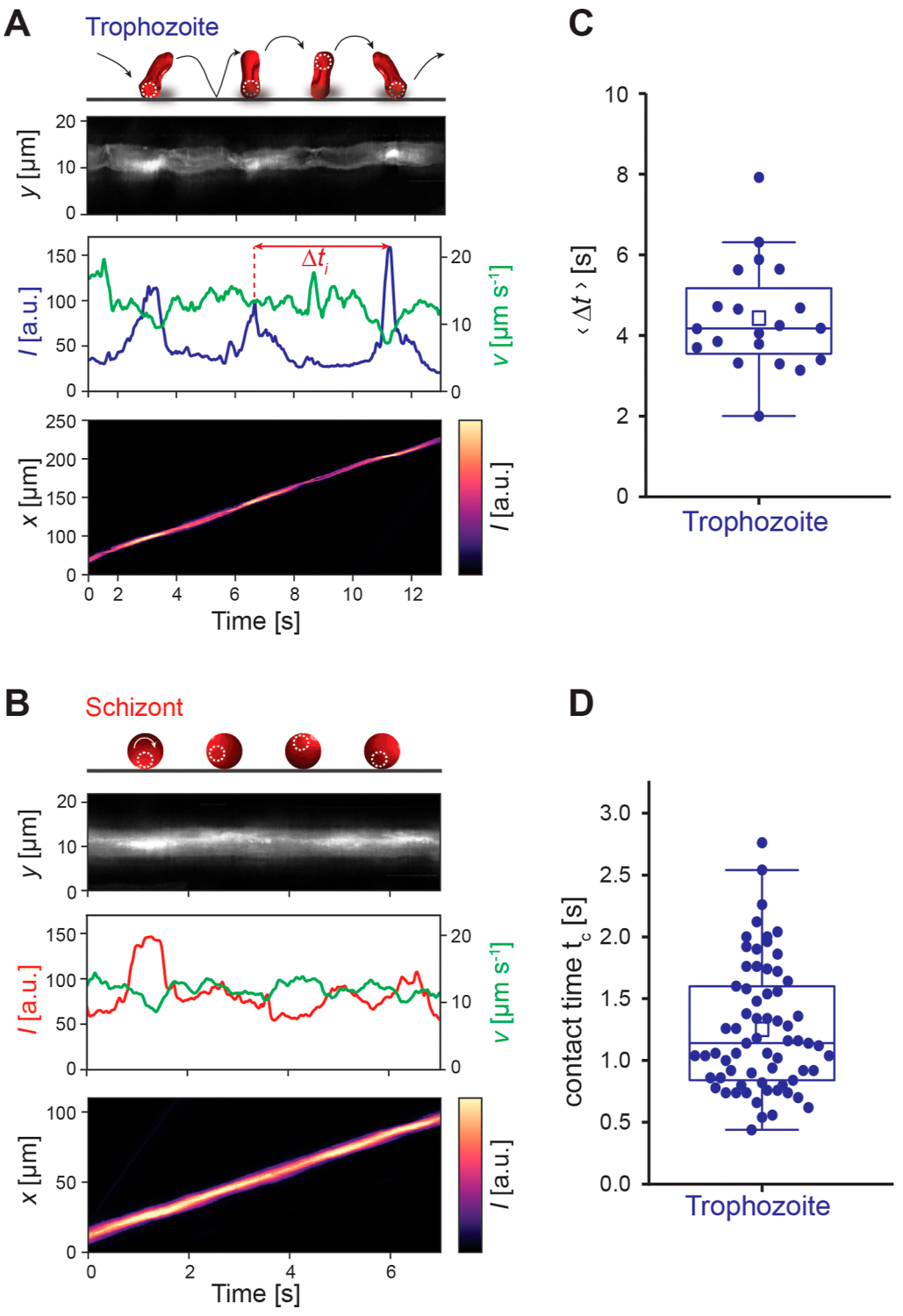

Figure 6. Temporal patterns of cell−surface contact and velocity. (A) Trophozoite: top to bottom—schematic of flipping trophozoite. Maximum intensity projection, intensity (I, blue) and translational velocity (v, green) over time, and corresponding RICM kymograph. Periodic high-intensity signals indicate regular flipping cycles. (B) The corresponding data of a rolling schizont (C) Rotation periodicity in trophozoites: mean $\langle \Delta t \rangle = 4.4 \pm 1.3$ s. (D) Mean contact time for trophozoites $\langle t_c \rangle = 1.3 \pm 0.5$ s. (box plot; each point is an independent biological replicate; see Materials and Methods for details).

intensity baseline (10%). In some cases, the velocity dropped to zero (e.g., at $t \approx 4.5$ and 9 s in Figure S4A), indicating transient pinning events that interrupted the flipping motion. Such pinning events lasted approximately 1 s. In summary, the periodic intensity peaks observed for trophozoites both in space (Figure 5A) and time (Figure 6A) are consistent with their discocyte-like shape and their off-centered digestive vacuole, which rotates with the flipping cell.

These periodic signatures were absent in the schizont traces (Figures 5B and 6B), suggestive of continuous rolling. Like trophozoites, schizont-stage infected erythrocytes occasionally transited from rolling to pinning and eventually to stationary

https://doi.org/10.1021/acsinfecdis.5c00594
ACS Infect. Dis. XXXX, XXX, XXX−XXX

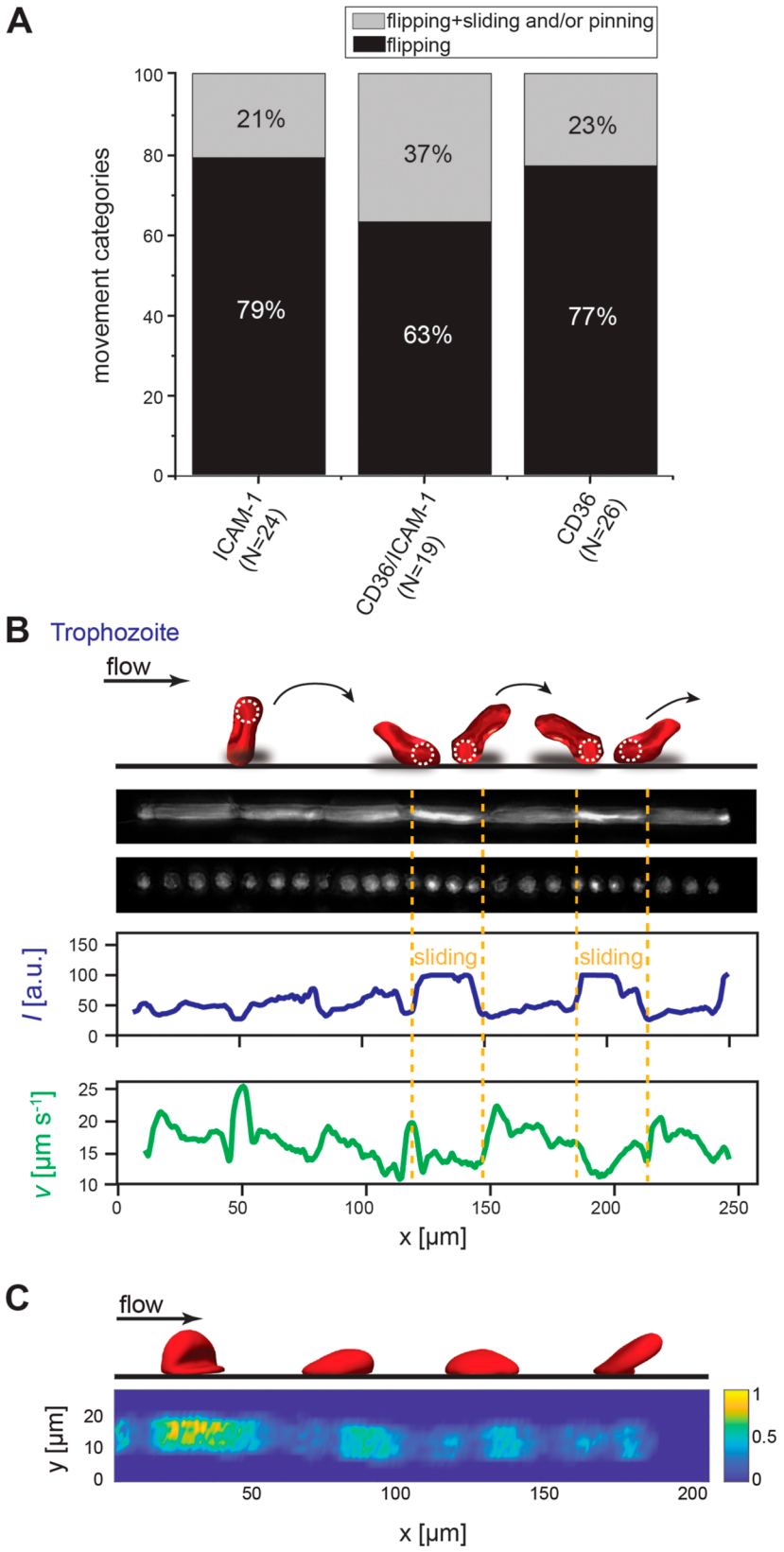

Figure 7. Adhesion dynamics of trophozoite-stage infected erythrocytes on different receptor-functionalized surfaces. (A) Proportions of motion types (pure flipping, flipping with sliding, etc.) on ICAM-1, ICAM-1/CD36, and CD36-only surfaces (Tables S1−S3). (B) Top to bottom - schematic of a flipping and sliding trophozoite on a mixed ICAM-1/CD36 surface (dashed circle marks digestive vacuole); maximum intensity projection of HS-RICM data; HS-RICM snapshot sequence; intensity (I, blue) and velocity (v, green) plotted over distance. Sliding phases are marked by plateaus in intensity and velocity (yellow dashed lines). (C) Top: simulation snapshots of a trophozoite flipping and sliding at high shear stress (~0.2 Pa) on a mixed-receptor surface with differential bond strengths (on/off rates: 17$\dot{\gamma}$ and 8.5$\dot{\gamma}$). Bottom: corresponding simulated contact footprint showing extended sliding zones.

https://doi.org/10.1021/acsinfecdis.5c00594
ACS Infect. Dis. XXXX, XXX, XXX−XXX

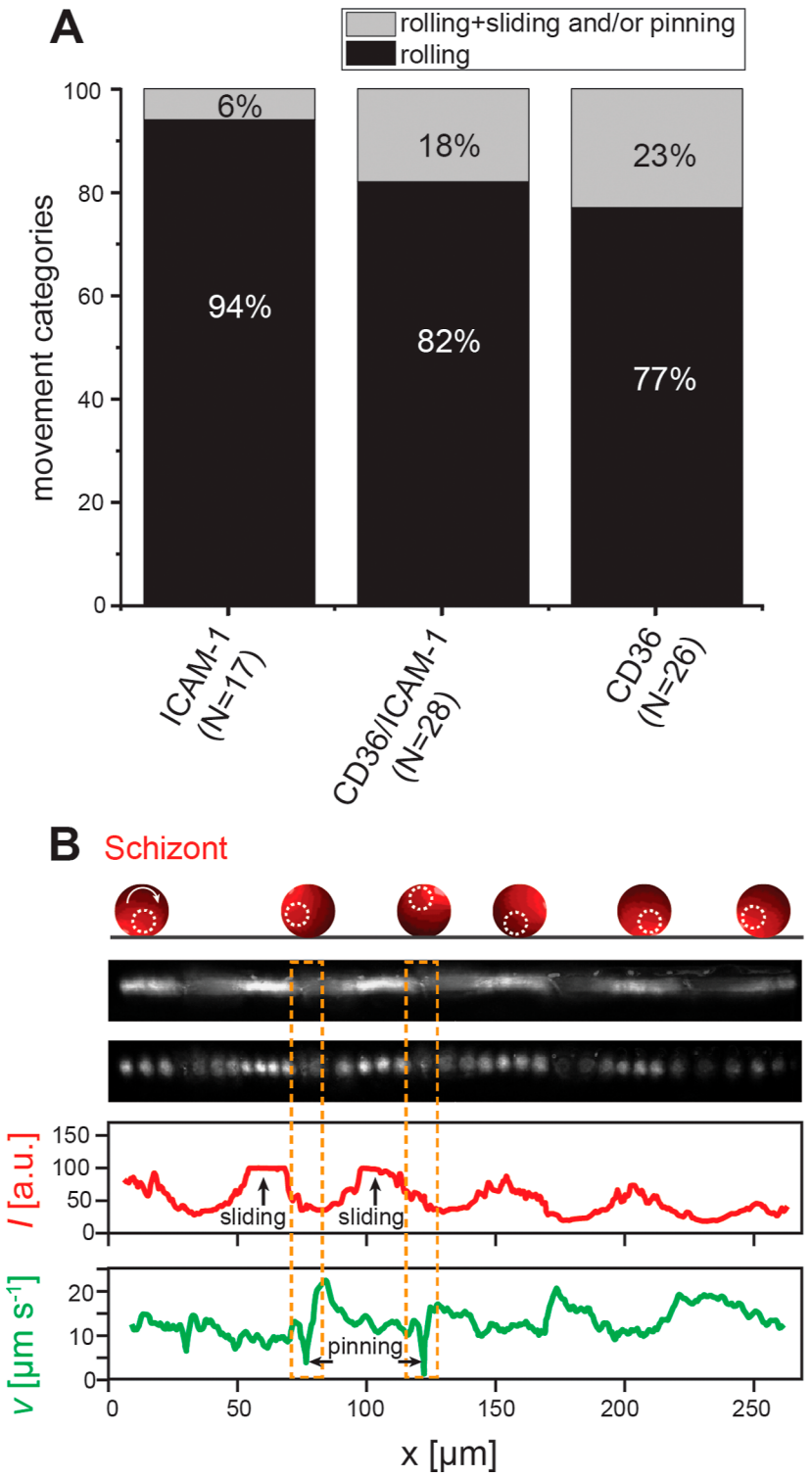

Figure 8. Adhesion dynamics of schizont-stage infected erythrocytes on different receptor-functionalized surfaces. (A) Distribution of motion types (rolling, rolling with sliding or pinning) for schizonts on ICAM-1, ICAM-1/CD36, and CD36-only substrates (Tables S4−S6). (B) Top to bottom -schematic of a schizont exhibiting rolling, sliding, and pinning (dashed circle marks the digestive vacuole); maximum intensity projection of HS-RICM images; representative HS-RICM snapshot sequence; signal intensity (I, red) and translational velocity (v, green) plotted over distance. Sliding phases (black arrows) correspond to intensity plateaus; pinning events are marked by sharp drops in velocity, highlighted by yellow dashed lines and black arrows.

adhesion (Figure S4B), as indicated by a high signal intensity, a decrease in velocity, and a lower slope in the kymogram (Figure S4B). The generation of such strong pinning centers both for trophozoites and schizonts can be attributed to the accumulation of ligand−receptor pairs on the fluid supported membranes under shear stress.[37]

Increased Sliding of Trophozoites on CD36-Functionalized Substrates. We next investigated the dynamic adhesion

https://doi.org/10.1021/acsinfecdis.5c00594
ACS Infect. Dis. XXXX, XXX, XXX−XXX

behavior of *P. falciparum*-infected erythrocytes on supported lipid membranes functionalized with either CD36 alone or a 1:1 mixture of ICAM-1 and CD36 (each at an intermolecular distance $\langle d \rangle$ = 11 nm between receptors). CD36 is a well-established endothelial receptor for cytoadherence and is coexpressed with ICAM-1 on various microvascular endothelial cell types, including human dermal microvascular endothelial cells (HDMECs).[23] Prior studies have shown that CD36 and ICAM-1 can act synergistically to enhance cytoadhesion.[24] Although CD36 was initially characterized as a receptor mediating stationary adhesion,[32] subsequent work has revealed that infected erythrocytes can also roll over CD36-presenting surfaces, including HDMEC monolayers.[23,27,39]

For these experiments, we used a previously described FCR3 parasite population selected on HDMECs, which predominantly expresses var. genes of the UpsB and UpsC subgroups, known to mediate binding to ICAM-1 and CD36.[22] Among the cells exhibiting dynamic adhesion behavior, approximately 63% of trophozoites flipped on the mixed substrate, a reduction compared to 79% flipping observed on the ICAM-1-only surface (Figure 7A). Notably, the mixed substrate also promoted a more complex behavior, with 37% of trophozoites showing combined flipping and extensive lateral sliding with or without pinning, compared to 21% on ICAM-1 alone (Figure 7A,B; Movie S3). Sliding is characterized by plateaus of high intensity and decreased velocity (Figure 7B), whereas pinning is a form of stationary adhesion, as evidenced by a velocity of zero. On CD36-only substrates, we also observed comparable incidences of pure flipping (77%) and flipping accompanied by sliding and pining (23%) (Figure 7A; Movie S4).

To support these experimental findings, we extended our computer simulations to include mixed ICAM-1/CD36 surfaces. The simulations, which accounted for differential receptor distribution and bond kinetics, confirmed that the presence of CD36 increases the level of lateral sliding on mixed substrates once trophozoites make contact with the surface following a flip (Figure 7C).

Schizont-infected erythrocytes consistently exhibited rolling behavior across all tested substrates (Figure 8). However, the proportion of cells displaying pure rolling decreased in the presence of CD36, whereas the proportion of cells displaying rolling combined with sliding and/or pinning increased compared to a pure ICAM-1 surface (Figure 8, Movies S5 and S6).

All HS-RICM experiments were conducted at 37 °C with a hematocrit of 0.01%. This ensured that conditions were comparable for all cells and gave good statistics. Attempts to increase the hematocrit to physiological values resulted in signal loss due to overcrowding near the substrate and the inability to track individual infected erythrocytes over time (Movie S7).

DISCUSSION

This study aims to gain quantitative insights into the adhesion dynamics of *P. falciparum*-infected erythrocytes. The ability of infected erythrocytes to cytoadhere and hence sequester in the microvasculature is a key evolutionary strategy of the parasite to escape splenic clearance mechanisms. To address the dynamic nature of cytoadhesion in controlled systems, we employed a DNA-based molecular adhesion footprint assay and HS-RICM. Combined with computer simulations, these two simplified but quantitative approaches revealed distinct adhesion patterns for trophozoites and schizonts. While we acknowledge that cytoadhesion in vivo is influenced by multiple factors, including temperature, hematocrit, wall shear stress, receptor composition, and surface topography[24,32,52,53]—not to mention parasite factors such as knob density, adhesin variant, and rosette formation[18,20,54,55]—the controlled experimental conditions used here allowed us to characterize adhesion dynamics with high spatial and temporal resolution.

The molecular adhesion footprint assay visualizes the spatial distribution of contact points via molecular force sensors known as TGTs.[43,45,46,56] Originally developed to probe integrin-ligand forces during cell adhesion, TGTs have since been applied to processes such as focal adhesion maturation, cadherin-mediated binding, T-cell receptor engagement, and force mapping in motile cells.[45,57−59] Their ability to retain force history, allow ligand internalization, and provide high signal-to-noise ratios enabled the development of foot printing assays to study rolling adhesion of leukocytes and cancer cells under flow.[43,57,60] In our adaptation, we functionalized PEG-coated microfluidic channels with chimeric Fc-ICAM-1 linked to an 18-mer DNA duplex and visualized adhesion footprints using a fluorescent DNA probe.

The adhesion footprints of trophozoites exhibited a periodic, patchy pattern characterized by regions of high fluorescence intensity interspersed within a broader band of diffuse, lower-intensity signals. Fluorescence intensity reflects the number of productive adhesion events, though it can also be modulated by the bond loading rate.[43,57] To interpret the footprints, we primarily focused on event density, assuming that each erythrocyte experiences comparable hydrodynamic conditions under the controlled shear flow and low hematocrit used in our setup.

This interpretation, however, does not account for the variability in the loading history of the individual bonds. In earlier studies involving spherical microparticles rolling in flow chambers, it was shown that molecular properties could be decoupled from other effects by incorporating particle geometry and loading trajectories.[57] In our case, this level of deconvolution is not feasible due to the biological complexity of the system. Infected erythrocytes, particularly at the trophozoite stage, exhibit asymmetric and heterogeneous shapes and variable mechanical and receptor properties, introducing variability in contact geometry and bond loading. For these reasons, we interpret the fluorescence intensity primarily as a spatial map of accumulated adhesion events while acknowledging that loading conditions may modulate the signal to some extent.

Nevertheless, our computer simulations partially account for these complexities by modeling flow conditions, cell deformability, and the slip-bond behavior of receptor−ligand pairs. These simulations incorporate the effect of loading rate at the molecular level,[51] providing a complementary perspective on the mechanical processes underlying the observed adhesion patterns.

The patch footprint pattern observed for trophozoites contradicts a continuous rolling model and instead supports a flipping motion over the substrate (Figure 2A−D). Computer simulations further corroborate this flipping behavior. However, the presence of diffuse, low-density contacts in areas above, below, and between high-density contact zones suggests the presence of additional contact events while flipping (Figure 2F,G).

The orientation of healthy red blood cells in flow is determined by the shear rate, as observed in capillary blood flow and microfluidic experiments.[61] At low shear rates, red blood cells tumble and flip over their long axis with their disk

https://doi.org/10.1021/acsinfecdis.5c00594
ACS Infect. Dis. XXXX, XXX, XXX−XXX

plane perpendicular to the flow.[61] In contrast, at higher shear stress, cells align their disk plane parallel to the flow, and flipping transitions to rolling.[61] Given that trophozoites largely retain the biconcave, discoid shape of healthy erythrocytes, but with a stiffer membrane,[14] they could potentially flip or jump over the short axis (like a rolling wheel) or the long axis (face-overface, like a flipping coin) (Figure 3). If trophozoites flip over the short axis (rolling along the rim), only a small portion of the membrane would be in contact at any given time, resulting in narrower and more linear contact footprints. However, this scenario does not align with the observed 6 μm footprint width, as rolling or jumping along the rim would produce a much smaller contact width (~2.5 μm), corresponding to the rim thickness. Furthermore, the center-to-center spacing of adhesion patches (i.e., high adhesion areas) (~18 μm) would be difficult to explain, as rolling would likely lead to continuous contact rather than discrete patches. In contrast, if trophozoites flip over their long axis, different regions of the broad cell surface alternatively engage and disengage with the substrate. The fact that the footprint width (~6 μm) closely matches the trophozoite diameter (~7−8 μm) strongly suggests that a large portion of the cell is making contact during each flipping cycle.

Our computer simulations confirmed the flipping of trophozoites over their long axis. Additionally, computer simulations revealed that the wall shear stress modulates the adhesion pattern. At low wall shear stress, trophozoite-stage erythrocytes encounter the surface face down, creating a donut-like shaped footprint (Figure 2F). At higher wall shear stress, the footprints became less regular, the number of high-density contact patches decreased, and some patches exhibited lateral extensions in both directions (Figure 2G), indicative of slipping or crawling. The differences in the contact footprints are explained in part by the wall shear stress affecting cell morphology. At low shear stress, the cell experiences minimal deformation, and because of their discoidal shape, the face-down encounter with the surface occurs primarily along their outer rim, producing the characteristic donut-shaped footprint. In contrast, high shear stress leads to significant cellular deformation, as shown by the simulated cell snapshots of trophozoites (Figure 2G).

Interestingly, the computer simulations could not fully explain the experimentally observed broad range of motion patterns, including the fact that the overall footprint tended to be as wide as the cell diameter. This indicates that processes not present in the computer simulations are important, including hotspots in adhesion, a possible detachment of the membrane from the cytoskeleton, and the inner structure of the infected erythrocyte, which in the trophozoite state is not uniformly filled yet with parasite mass. Corresponding models do not exist yet and must be developed in the future to better understand the underlying mechanisms.

HS-RICM provided complementary insights. Unlike the DNA force sensor assay, where ICAM-1 molecules are immobilized by molecular anchors, the supported lipid membranes used for HS-RICM analysis allow lateral mobility of adhesion receptors,[36,37] better mimicking the physiological conditions of cytoadhesion to the endothelium. Although the precise detection of the adhesion footprints was not possible due to the strong light scattering from the parasite,[37] the RICM signal intensity provided spatiotemporal insights. The spatial pattern of the adhesion contacts of trophozoites appeared to be similar to those obtained by the adhesion footprint assay, showing peaks corresponding to moments when the parasite vacuole is close to the surface during flipping. HS-RICM further supports the model that trophozoites flip over their long axis in flow and not the short axis. Additionally, the observation that trophozoites rotate and tumble during both flipping and attachment provides a plausible explanation for the specific contact points with the substrate beyond the high adhesion areas.

HS-RICM also provided additional temporal information. For example, the analysis of the integrated intensity plotted as a function of time (Figure 6A) yielded the mean periodicity of rotation ($\langle \Delta t_i \rangle$ = 4.4 ± 1.3 s) and the lifetime of cell−surface contacts ($\langle t_c \rangle$ = 1.3 ± 0.5 s) on ICAM-1 functionalized supported membranes for trophozoites.

HS-RICM analysis further revealed that trophozoite-stage infected erythrocytes also exhibit flipping behavior on supported membranes functionalized with CD36 or with a combination of CD36 and ICAM-1, albeit with notable differences in adhesion dynamics. Specifically, the proportion of cells undergoing pure flipping decreased on the mixed-receptor surfaces, while the fraction displaying flipping combined with lateral sliding, with or without transient pinning, increased compared to substrates presenting only one receptor (Figure 7A). Computer simulations align with the experimental data, revealing a flipping/sliding motion phenotype on the mixed substrate (Figure 7C).

These changes in dynamic contact phenotypes are consistent with the distinct bond mechanics of the two receptors. ICAM-1 forms catch bonds with PfEMP1, where bond lifetimes increase under moderate force, thereby stabilizing discrete, prolonged contacts.[31] In contrast, CD36 engages in multiple slip bonds, characterized by decreasing bond lifetime with increasing force.[31] Notably, the association rate of CD36 is approximately 10-fold higher than that of ICAM-1, despite both having comparable dissociation constants.[31] This combination of faster binding and force-sensitive dissociation likely facilitates more transient sliding interactions on the mixed surface, contributing to the altered adhesion phenotype observed. Additionally, the lateral mobility of the receptors in the supported bilayers might also contribute to sliding.

Based on these findings, we propose the following mechanism for trophozoite adhesion and movement in flow: trophozoites travel with their broad disk side facing the shear stress, while undergoing a tumbling motion. Initial contact with the surface likely occurs at the edge between the small and broad sides of the cell. Once adhesion bonds are formed, the cell's free motion is constrained, and the wall shear stress presses the cell face down onto the support, promoting additional interactions with the support beyond the initial adhesion zone. Shear stress also induces lateral sliding or crawling, leading to variable adhesion footprints before detachment. The cell then flips over its long axis, re-establishing contact at a site opposite the previous adhesion zone, and the cycle repeats (Figure 2A).

In contrast to trophozoites, schizonts exhibited a simple, uniform adhesion footprint typical of a spherical cell with a stiff membrane, indicating a rolling motion (Figure 4A). Computer simulations, which accounted for the spherical geometry and increased membrane stiffness of schizonts, reproduced the experimental findings and confirmed a rolling behavior under flow (Figure 4F,G). Likewise, the HS-RICM imaging revealed continuous, homogeneous contact patterns (Figure 5B), further corroborating the interpretation of stable rolling across the substrate.

https://doi.org/10.1021/acsinfecdis.5c00594
ACS Infect. Dis. XXXX, XXX, XXX−XXX

Unlike trophozoites, schizonts also did not exhibit periodic changes in intensity and velocity; however, friction-induced reductions in translational velocity were inferred from anticorrelated fluctuations in intensity $I(t)$ and velocity $v(t)$. Notably, real-time HS-RICM imaging also captured transient transitions in movement, including switches from rolling to sliding and occasionally pinning, likely driven by dynamic rearrangements of ligand−receptor interactions (Figure S4). Importantly, rolling remained the predominant adhesion phenotype for schizonts across all substrates tested, ICAM-1, CD36, and the ICAM-1/CD36 mixture (Figure 8A). However, there was an increase in the subpopulation displaying combined rolling and lateral sliding with or without transient pinning on substrates containing CD36 (Figure 8A).

Previous studies have shown that the interaction with infected erythrocytes can activate the endothelial cells, resulting in upregulation of surface receptors, such as ICAM-1 and CD36, which in turn promote further binding of infected erythrocytes.[22−25] Our study suggests that the contact between an infected erythrocyte and an endothelial cell is not limited to a single point but can extend along the entire length of the microvascular endothelial cell. Considering that an endothelial cell is roughly 50−70 μm long and 10−30 μm wide[62] and given that both the DNA footprint assay and the HS-RICM analysis showing significantly longer tracks, a single infected erythrocyte can come into contact with a large section of the luminal surface area of an endothelial cell during dynamic adhesion motion. Such motion likely exerts significant mechanical stress, promoting endothelial activation. In summary, our findings suggest that the dynamic motion patterns of infected erythrocytes over the endothelial lining are a critical factor that cannot be ignored and likely contribute to the pathology of falciparum malaria.

MATERIALS AND METHODS

***P. falciparum* Cell Culture.** *P. falciparum* line FCR3 was cultured as described[22] and synchronized using 5% sorbitol.[63] Prior to the adhesion assays, FCR3 was repeatedly panned on Petri dishes coated with ICAM-1 to select for an ICAM-1 binding population or on HDMECs to select for a population cytoadhering to both ICAM-1 and CD36. HDMECs present both CD36 and ICAM-1.[24] The HDMEC-selected FCR3 population has recently been characterized and was shown to express IT4var13, IT4var25, and IT4var66, which are predicted to confer binding to ICAM-1 and/or CD36.[22] Trophozoites and schizonts were enriched from highly synchronized cultures using the magnet cell sorting method.[64] The cell density was determined using a cell counter (Beckman Coulter) and adjusted to 2×10^6 cells mL^{-1} in binding medium (RPMI 1640 without glutamate adjusted to pH = 7.4 using $K_2(CO_4)$).

Preparation of the DNA Force Sensor Assay. The surface functionalization for the DNA force sensor assay was adapted from Li et al. (2017) and followed a multistep process.[43] (i) Assembly and passivation of channels: glass slides were incubated with 3-aminopropyltriethoxysilane (APTES, 1:100 in ethanol) for 1 h at room temperature (RT), washed with ethanol, dried with nitrogen gas, and stored at −20 °C until further use. The glass slide was subsequently glued to bottomless Ibidi μ-slide channels (Ibidi, μ-slide VI0.4) using polydimethylsiloxane. To passivate the activated glass and block nonspecific adhesion, a mixture of PEG5000-NHS and MAL-PEG5000-biotin (1:100, 2 mg mL^{-1}, LaysanBio) was added for 2 h at RT. After washing the channel with PBS, neutravidin (500 μg mL^{-1}) was added for 1 h at RT to saturate all biotin molecules and to serve as anchor points for the DNA sensor. (ii) Preparation of force sensors: protein G (1 mg mL^{-1}, Abcam) was incubated with SMCC (sulfosuccinimidyl 4-(*N*-maleimidomethyl) cyclohexan-1-carboxylat) cross-linker (2 mg, ThermoFisher Scientific) for 30 min at RT. The top oligonucleotide strand, containing a protected S−S−H group at the 3′ end (250 nM, 5′ GTG TCG TGC CTC CGT GCT GTG ThioMC3-D 3′, IDT Technologies), was incubated with Tris(2-chlorehyl) phosphate (TCEP) for 20 min, followed by centrifugation at 13,000*g* for 10 min using a centrifugation column (Miltenyi). The protein G and top oligonucleotide strand solutions were combined and allowed to react for 30 min at RT before adding the biotin-functionalized bottom oligonucleotide (250 nM, 5′ Bio GTT TTT TTC ACA GCA CGG AGG CAC GAC AC 3′). The mixture was then incubated at 65 °C for 5 min to allow the strands to anneal. The mixture was subsequently added to each channel and incubated for 2 h at RT or overnight at 4 °C to attach the sensor to the channel surface via the interaction of biotin with neutravidin. Finally, chimeric Fc-ICAM-1 (100 μg mL^{-1}) was added to the channels and incubated for at least 1 h at RT. The channels were washed with PBS to remove any unbound components. (iii) Verification: to verify each step, fluorescent probes were used as follows: IgG-Alexa 488 (1:100, Invitrogen) to detect protein G, Streptavidin-Alexa647 (Invitrogen) to detect biotin, and a complementary oligonucleotide with Atto-647 (IDT Technologies) to determine the annealing of the strands and their anchoring to the substrate. Imaging was performed using an AxioObserver Z1 inverted microscope (Zeiss).

DNA Force Sensor Assay. 200 μL of infected erythrocytes (2×10^6 cells mL^{-1}) in 37 °C prewarmed binding media were allowed to settle onto the ICAM-1 functionalized surface for 5 min before a wall shear stress of 0.1 Pa was applied for 5 min, using a syringe pump (World Precision Instruments). The experiment was performed in an incubation chamber with an ambient temperature of 37 °C. The unzipped DNA strands (footprints) were subsequently detected by adding a solution containing 300 nM complementary oligonucleotide conjugated with Atto647/Cy3 (IDT Technologies) for 1 h. The channel was subsequently washed, and the resulting footprint was observed under a VisitronSystems TIRF microscope based on an AxioObserver Z1 microscope (Zeiss) equipped with a 100× Objective (Zeiss, NA 1,46) and a Hamamatsu EMCCD 9100−50 camera (pixel size 8 μm). The TIRF filter settings were 546 E_x/E_m: 513/580 nm or 647 E_x/E_m: 615/660 nm. To confirm the specificity of the cytoadhesion of *P. falciparum* infected erythrocytes, we performed negative control experiments using uninfected erythrocytes. For each experimental condition, the fluorescence signals were recorded in at least 6 different fields across the channel.

Image Analyses—DNA Force Sensor Assay. We wrote a customized code, yielding values for the length, width, center-to-center distance between patches and area of the patches. Track width: for each image, we calculated the average intensity profile along the *x*-axis (the track path). Typically, this profile exhibited a peak near the midwidth, gradually decreasing toward a background fluorescence intensity of ∼20. Track width was estimated by setting an intensity threshold and identifying its intersections with the average intensity profile. This process was repeated at each x-value along the track, with intensity profiles smoothed using a 21-pixel bin (±10 pixels). Near the image edges (x < 10 or x > end point-10), a 5-pixel bin (±2 pixels) was

https://doi.org/10.1021/acsinfecdis.5c00594
ACS Infect. Dis. XXXX, XXX, XXX−XXX

used for smoothing. Unrealistic deviations (>5 pixels from previous points) were discarded, allowing for precise measurement of track width variations.

Intensity autocorrelation: to analyze periodicity, we first averaged intensity values along the y-axis for each x-value, obtaining an intensity profile $I(x)$. The spatial autocorrelation function was then computed as

$$C(s) = \sum_x [(I(x) - I_{mean})\cdot(I(x+s) - I_{mean})]$$

where I_{mean} is the mean intensity, and s ranges from 0 to 400 pixels. The normalized autocorrelation was defined as

$$C(s) = \frac{C_{(s)}}{C_{(0)}}$$

The second peak of the autocorrelation function defined the periodicity of the spatial pattern. To create a 3D projection on a cylindrical surface with a 7.2 μm mean diameter and an average circumference of 22 μm, we first wrapped the track image onto itself at every periodic separation (estimated from autocorrelation profiles) to create an average track. Then, the average track image was stitched to complete the surface at the point of minimum intensity, which avoided any discontinuity.

Patch Size: patch identification was performed using the SciPy *ndimage* module. A fluorescence intensity threshold of 150 nm was applied to filter out low-intensity regions. Connected components were labeled using *ndimage.label*, with each component representing a distinct patch. Patches smaller than 50 pixels in width or 1 pixel in height were excluded. This method allowed for the accurate segmentation and characterization of high-intensity fluorescence patches for further analysis.

Real-Time Imaging of Dynamic Adhesion Contacts with HS-RICM. The surface was functionalized as described.[37] Briefly, a cleaned glass slide was bonded to a bottomless flow chamber (ibidi). The chamber was then filled with a suspension of vesicles containing 0.5 mol % of NTA lipids (Avanti Polar Lipids). After removal of excess vesicles by intensive rinsing, the supported membrane surface was functionalized with histidine-tagged ICAM-1, CD36, or 1:1 mixture of both (ACROBiosystem and Thermo Fisher Scientific). The average intermolecular distance between receptor molecules was $\langle d \rangle$ = 11 nm.[37] The microfluidic chamber was mounted onto an Axio Observer Z.1 inverted microscope (Zeiss). The sample was illuminated with a monochromatic, linearly polarized light (λ_{EX} = 546 nm).[65,66] Images were acquired using a FastCam Mini AX50 high-speed camera (VKT Video Kommunikation GmbH) at a frame rate of 250 fps. The cell suspension (10^6 cells mL^{-1} in 37 °C prewarmed binding media) was allowed to react with the functionalized supported membranes at a constant shear stress of 0.03 Pa throughout the experiments. 50−80% of the cells were moving over the substrate.

Image Analysis—HS-RICM. The images captured by HS-RICM were analyzed by using a self-written pipeline. The intensity collected from each pixel was median-averaged across five consecutive frames, followed by background subtraction. The region of interest (ROI) was defined as the 400 brightest pixels from each adhesion contact, which were blurred by a Gaussian filter. The signal intensity from each ROI was determined by averaging the intensities of the five brightest pixels. The position of the cell at each time point was defined as the position of the center of mass of the corresponding ROI. The temporal velocity was calculated from the displacement of the center of mass over 70 frames, corresponding to 0.28 s.

Computer Simulations of Footprints. The footprints of trophozoites and schizonts were simulated using a deformable red blood cell model and multiparticle collision hydrodynamics, as previously described.[22] Mesoscopic simulations include adhesion dynamics of deformable red blood cells on a substrate in a shear flow. Hydrodynamics is implemented using multiparticle collision dynamics.[67,68] It consists of solvent particles with mass m organized into cubic grid cells of a side length of a within a simulation box. Both mass m and grid size a set the mass and length scales in the system. Solvent particle positions evolve via streaming step and velocities evolve via collision step which is the momentum exchange step among solvent particles. The streaming step is

$$r_i(t + \Delta t) = r_i + v_i(t)\Delta t$$

where Δt is collision time step and $v_i(t)$ is the velocity of the particle i at time t. The collision step is

$$v_i(t + \Delta t) = v_{cm}(t) + R(\alpha)(v_i(t) - v_{cm}(t))$$

where $v_{cm}(t)$ is the center of mass velocity of the grid cell to which particle i belongs and $R(\alpha)$ is stochastic rotation matrix for which angle of rotation α = 135° is fixed for the whole simulation. The solvent density ρ = 10, angle of rotation α, and collision time step Δt = 0.02 set solvent viscosity.

The red blood cell is modeled as a two-dimensional triangular meshwork of nodes connected by springs. The number of nodes is chosen to be N = 1000. For full model details, please refer to ref 22,49, and 69. For modeling trophozoites, a discocyte shape is chosen with shear modulus σ_0 = 30 μNm^{-1} and bending rigidity is set to $\kappa_b = 5.7 \times 10^{-19}$ J, whereas for schizonts, spherical shape is chosen with shear modulus σ_0 = 50 μNm^{-1} and bending rigidity of $\kappa_b = 6.2 \times 10^{-19}$ J. Adhesion dynamics is implemented between the membrane vertices and the ligands that are distributed on the substrate. As described in earlier work,[22] bond association occurs with a constant on-rate κ_{on} and bond dissociation occurs with forces depending on off-rate κ_{off} according to Bell's law.[70] The bond association and dissociation probabilities are $P_{on} = 1 - \exp(-\kappa_{on}\Delta t_{md})$ and $P_{off} = 1 - \exp(-\kappa_{off}\Delta t_{md})$, respectively. The force on the existing receptor−ligand is $F(l) = k_s(l - l_0)$, where spring constant k_s is chosen to be 25.7×10^{-5} Nm^{-1} and l_0 is chosen to be 40 nm. The critical distance for bond formation is 280 nm. Both on and off-rates are set at $0.5\dot{\gamma}$, where $\dot{\gamma}$ is the shear rate. The range of shear stress used in the simulations is 0.04−0.12 Pa. To convert time scales in model units to physical units, solvent viscosity is assumed to be 1 mPas. For recapitulating flipping and sliding behavior by trophozoites, we performed simulations at large shear stress of ≃0.2 Pa and on and off-rates are set at $17\dot{\gamma}$ and $8.5\dot{\gamma}$, respectively. The substrate is also coated with two different ligands with spring constants k_s and $2k_s$, respectively. High shear ensures sufficient cell deformation, while the elevated on-rate maintains adhesion during sliding without detachment.

Statistical Analysis. Statistical analysis was performed using Origin Pro 2020 (OriginLab, Northampton, MA, USA) and Scipy,[71] employing either a Mann−Whitney U test or Student's t-test; p-values <0.01 were considered significant. The standard deviation is provided throughout. All boxplots presented in this study present the median value as a solid line and the average value as a square. The boxes correspond to the 25−75 percentile ranges, and the whiskers correspond to the 5−95 percentiles.

https://doi.org/10.1021/acsinfecdis.5c00594
ACS Infect. Dis. XXXX, XXX, XXX−XXX

■ ASSOCIATED CONTENT

Data Availability Statement

The data underlying this study are available in the published article and its online Supporting Information. The codes used for computer simulations are available at https://github.com/AnilBiophysics/Adhesion_Dynamics_iRBC.

Supporting Information

The Supporting Information is available free of charge at https://pubs.acs.org/doi/10.1021/acsinfecdis.5c00594.

Production of DNA force sensor; footprint tracks; extended analysis of footprint parameters; extended analysis of translational movements; snapshots of RICM images; and categorization of trophozoite and schizont motion behavior over various surfaces (PDF)

Representative HS-RICM of a trophozoite flipping over ICAM-1 (AVI)

Representative HS-RICM of a schizont rolling over ICAM-1 (AVI)

Representative HS-RICM of a trophozoite flipping and sliding on an ICAM-1/CD36 functionalized supported membrane (AVI)

Representative HS-RICM of a trophozoite flipping over CD36 (AVI)

Representative HS-RICM of a schizont rolling and pinning on an ICAM-1/CD36 functionalized supported membrane (AVI)

Representative HS-RICM of a schizont rolling over CD36 (AVI)

Representative HS-RICM of cells with a hematocrit of 2.0% and a parasitemia of 3% (AVI)

■ AUTHOR INFORMATION

Corresponding Authors

Ulrich S. Schwarz − *Heidelberg University, Institute for Theoretical Physics, 69120 Heidelberg, Germany;* orcid.org/0000-0003-1483-640X; Email: schwarz@thphys.uni-heidelberg.de

Motomu Tanaka − *Heidelberg University, Institute for Physical Chemistry, Physical Chemistry of Biosystems, 69120 Heidelberg, Germany; Kyoto University, Center for Integrative Medicine and Physics, 606-8502 Kyoto, Japan;* orcid.org/0000-0003-3663-9554; Email: tanaka@uni-heidelberg.de

Michael Lanzer − *Heidelberg University, Medical Faculty, Centre of Infectious Diseases, Parasitology, 69120 Heidelberg, Germany;* orcid.org/0000-0002-0220-6526; Email: Michael.Lanzer@med.uni-heidelberg.de

Authors

Katharina Scholz − *Heidelberg University, Institute for Physical Chemistry, Physical Chemistry of Biosystems, 69120 Heidelberg, Germany*

Marianne Papagrigorakes − *Heidelberg University, Medical Faculty, Centre of Infectious Diseases, Parasitology, 69120 Heidelberg, Germany*

Leon Lettermann − *Heidelberg University, Institute for Theoretical Physics, 69120 Heidelberg, Germany*

Federica Pennarola − *Max-Planck Institute for Medical Research, Cellular Biophysics, 69120 Heidelberg, Germany*

Pintu Patra − *Indian Institute of Technology, Department of Physics, Kharagpur 721302, India*

Anil Kumar Dasanna − *Indian Institute of Science Education and Research Mohali, Knowledge City 140306 Punjab, India;* orcid.org/0000-0001-5960-4579

Cecilia P. Sanchez − *Heidelberg University, Medical Faculty, Centre of Infectious Diseases, Parasitology, 69120 Heidelberg, Germany*

Jessica Kehrer − *Heidelberg University, Medical Faculty, Centre of Infectious Diseases, Parasitology, 69120 Heidelberg, Germany*

Elisabetta Ada Cavalcanti-Adam − *Max-Planck Institute for Medical Research, Cellular Biophysics, 69120 Heidelberg, Germany; University of Bayreuth, Cellular Biomechanics, 95447 Bayreuth, Germany*

Complete contact information is available at: https://pubs.acs.org/10.1021/acsinfecdis.5c00594

Author Contributions

M.L., U.S.S., M.T., and A.C.A. designed the study. K.S., M.P., C.P.S., and J.K. performed experiments. A.K.D. performed computer simulations. K.S., M.P., L.L, F.P., P.P., U.S.S., A.C.A., M.T., and M.L. analyzed results. U.S.S., M.T., and M.L. wrote the manuscript. All authors participated in discussion and manuscript editing.

Funding

This work was funded by the Deutsche Forschungsgemeinschaft (DFG, German Research Foundation)—project number 240245660-SFB 1129 (M.L., U.S.S, M.T. and A.C.A.).

Notes

The authors declare no competing financial interest.

■ ACKNOWLEDGMENTS

We acknowledge support from the Infectious Diseases Imaging Platform (IDIP) at the Center for Infectious Disease Research, Medical Faculty, Heidelberg University. We thank A. Kernaja and M. Müller for technical assistance. K.S. thanks J. Thoma and A. Yamamoto for supporting the optimization of the HS-RICM setup.

■ REFERENCES

(1) World Health Organization. *World Malaria Report 2024*; World Health Organization: Geneva, 2024.

(2) White, N. J.; Pukrittayakamee, S.; Hien, T. T.; Faiz, M. A.; Mokuolu, O. A.; Dondorp, A. M. Malaria. *Lancet* **2014**, *383* (9918), 723−735.

(3) Maier, A. G.; Cooke, B. M.; Cowman, A. F.; Tilley, L. Malaria parasite proteins that remodel the host erythrocyte. *Nat. Rev. Microbiol.* **2009**, *7* (5), 341−354.

(4) Cyrklaff, M.; Sanchez, C. P.; Kilian, N.; Bisseye, C.; Simpore, J.; Frischknecht, F.; Lanzer, M. Hemoglobins S and C interfere with actin remodeling in *Plasmodium falciparum*-infected erythrocytes. *Science* **2011**, *334* (6060), 1283−1286.

(5) Cyrklaff, M.; Srismith, S.; Nyboer, B.; Burda, K.; Hoffmann, A.; Lasitschka, F.; Adjalley, S.; Bisseye, C.; Simpore, J.; Mueller, A. K.; Sanchez, C. P.; Frischknecht, F.; Lanzer, M. Oxidative insult can induce malaria-protective trait of sickle and fetal erythrocytes. *Nat. Commun.* **2016**, *7*, 13401.

(6) Zhang, Y.; Huang, C.; Kim, S.; Golkaram, M.; Dixon, M. W.; Tilley, L.; Li, J.; Zhang, S.; Suresh, S. Multiple stiffening effects of nanoscale knobs on human red blood cells infected with *Plasmodium falciparum* malaria parasite. *Proc. Natl. Acad. Sci. U.S A.* **2015**, *112* (19), 6068−6073.

(7) Waldecker, M.; Dasanna, A. K.; Lansche, C.; Linke, M.; Srismith, S.; Cyrklaff, M.; Sanchez, C. P.; Schwarz, U. S.; Lanzer, M. Differential time-dependent volumetric and surface area changes and delayed

induction of new permeation pathways in *P. falciparum*-infected hemoglobinopathic erythrocytes. *Cell. Microbiol.* **2017**, *19* (2), No. e12650.
(8) Mauritz, J. M.; Esposito, A.; Ginsburg, H.; Kaminski, C. F.; Tiffert, T.; Lew, V. L. The homeostasis of *Plasmodium falciparum*-infected red blood cells. *PLoS Comput. Biol.* **2009**, *5* (4), No. e1000339.
(9) Sanchez, C. P.; Patra, P.; Chang, S. S.; Karathanasis, C.; Hanebutte, L.; Kilian, N.; Cyrklaff, M.; Heilemann, M.; Schwarz, U. S.; Kudryashev, M.; Lanzer, M. KAHRP dynamically relocalizes to remodeled actin junctions and associates with knob spirals in *Plasmodium falciparum*-infected erythrocytes. *Mol. Microbiol.* **2022**, *117* (2), 274−292.
(10) Watermeyer, J. M.; Hale, V. L.; Hackett, F.; Clare, D. K.; Cutts, E. E.; Vakonakis, I.; Fleck, R. A.; Blackman, M. J.; Saibil, H. R. A spiral scaffold underlies cytoadherent knobs in *Plasmodium falciparum*-infected erythrocytes. *Blood* **2016**, *127* (3), 343−351.
(11) Tilly, A.-K.; Thiede, J.; Metwally, N.; Lubiana, P.; Bachmann, A.; Roeder, T.; Rockliffe, N.; Lorenzen, S.; Tannich, E.; Gutsmann, T.; Bruchhaus, I. Type of in vitro cultivation influences cytoadhesion, knob structure, protein localization and transcriptome profile of *Plasmodium falciparum*. *Sci. Rep.* **2015**, *5* (1), 16766.
(12) Cutts, E. E.; Laasch, N.; Reiter, D. M.; Trenker, R.; Slater, L. M.; Stansfeld, P. J.; Vakonakis, I. Structural analysis of *P. falciparum* KAHRP and PfEMP1 complexes with host erythrocyte spectrin suggests a model for cytoadherent knob protrusions. *PLoS Pathog.* **2017**, *13* (8), No. e1006552.
(13) Helms, G.; Dasanna, A. K.; Schwarz, U. S.; Lanzer, M. Modeling cytoadhesion of *Plasmodium falciparum*-infected erythrocytes and leukocytes-common principles and distinctive features. *FEBS Lett.* **2016**, *590* (13), 1955−1971.
(14) Fröhlich, B.; Jäger, J.; Lansche, C.; Sanchez, C. P.; Cyrklaff, M.; Buchholz, B.; Soubeiga, S. T.; Simpore, J.; Ito, H.; Schwarz, U. S.; Lanzer, M.; Tanaka, M. Hemoglobin S and C affect biomechanical membrane properties of *P. falciparum*-infected erythrocytes. *Commun. Biol.* **2019**, *2*, 311.
(15) Cooke, B. M.; Mohandas, N.; Coppel, R. L. The malaria-infected red blood cell: structural and functional changes. *Adv. Parasitol.* **2001**, *50*, 1−86.
(16) Lavazec, C. Molecular mechanisms of deformability of Plasmodium-infected erythrocytes. *Curr. Opin. Microbiol.* **2017**, *40*, 138−144.
(17) Jäger, J.; Patra, P.; Sanchez, C. P.; Lanzer, M.; Schwarz, U. S. A particle-based computational model to analyse remodelling of the red blood cell cytoskeleton during malaria infections. *PLoS Comput. Biol.* **2022**, *18* (4), No. e1009509.
(18) Crabb, B. S.; Cooke, B. M.; Reeder, J. C.; Waller, R. F.; Caruana, S. R.; Davern, K. M.; Wickham, M. E.; Brown, G. V.; Coppel, R. L.; Cowman, A. F. Targeted gene disruption shows that knobs enable malaria-infected red cells to cytoadhere under physiological shear stress. *Cell* **1997**, *89* (2), 287−296.
(19) Wahlgren, M.; Goel, S.; Akhouri, R. R. Variant surface antigens of *Plasmodium falciparum* and their roles in severe malaria. *Nat. Rev. Microbiol.* **2017**, *15* (8), 479−491.
(20) Metwally, N. G.; Tilly, A. K.; Lubiana, P.; Roth, L. K.; Dörpinghaus, M.; Lorenzen, S.; Schuldt, K.; Witt, S.; Bachmann, A.; Tidow, H.; Gutsmann, T.; Burmester, T.; Roeder, T.; Tannich, E.; Bruchhaus, I. Characterisation of *Plasmodium falciparum* populations selected on the human endothelial receptors P-selectin, E-selectin, CD9 and CD151. *Sci. Rep.* **2017**, *7* (1), 4069.
(21) Lim, X. R.; Harraz, O. F. Mechanosensing by vascular endothelium. *Annu. Rev. Physiol.* **2024**, *86* (86), 71−97.
(22) Lansche, C.; Dasanna, A. K.; Quadt, K.; Fröhlich, B.; Missirlis, D.; Tétard, M.; Gamain, B.; Buchholz, B.; Sanchez, C. P.; Tanaka, M.; Schwarz, U. S.; Lanzer, M. The sickle cell trait affects contact dynamics and endothelial cell activation in *Plasmodium falciparum*-infected erythrocytes. *Commun. Biol.* **2018**, *1*, 211.
(23) Davis, S. P.; Amrein, M.; Gillrie, M. R.; Lee, K.; Muruve, D. A.; Ho, M. *Plasmodium falciparum*-induced CD36 clustering rapidly strengthens cytoadherence via p130CAS-mediated actin cytoskeletal rearrangement. *FASEB J.* **2012**, *26* (3), 1119−1130.
(24) Yipp, B. G.; Anand, S.; Schollaardt, T.; Patel, K. D.; Looareesuwan, S.; Ho, M. Synergism of multiple adhesion molecules in mediating cytoadherence of *Plasmodium falciparum*-infected erythrocytes to microvascular endothelial cells under flow. *Blood* **2000**, *96* (6), 2292−2298.
(25) Tripathi, A. K.; Sullivan, D. J.; Stins, M. F. *Plasmodium falciparum*-infected erythrocytes increase intercellular adhesion molecule 1 expression on brain endothelium through NF-kappaB. *Infect. Immun.* **2006**, *74* (6), 3262−3270.
(26) Carvalho, P. A.; Diez-Silva, M.; Chen, H.; Dao, M.; Suresh, S. Cytoadherence of erythrocytes invaded by *Plasmodium falciparum*: quantitative contact-probing of a human malaria receptor. *Acta Biomater.* **2013**, *9* (5), 6349−6359.
(27) Davis, S. P.; Lee, K.; Gillrie, M. R.; Roa, L.; Amrein, M.; Ho, M. CD36 recruits $\alpha_5\beta_1$ integrin to promote cytoadherence of *P. falciparum*-infected erythrocytes. *PLoS Pathog.* **2013**, *9* (8), No. e1003590.
(28) Li, A.; Lim, T. S.; Shi, H.; Yin, J.; Tan, S. J.; Li, Z.; Low, B. C.; Tan, K. S.; Lim, C. T. Molecular mechanistic insights into the endothelial receptor mediated cytoadherence of *Plasmodium falciparum*-infected erythrocytes. *PLoS One* **2011**, *6* (3), No. e16929.
(29) Xu, X.; Efremov, A. K.; Li, A.; Lai, L.; Dao, M.; Lim, C. T.; Cao, J. Probing the cytoadherence of malaria infected red blood cells under flow. *PLoS One* **2013**, *8* (5), No. e64763.
(30) Antia, M.; Herricks, T.; Rathod, P. K. Microfluidic modeling of cell-cell interactions in malaria pathogenesis. *PLoS Pathog.* **2007**, *3* (7), No. e99.
(31) Lim, Y. B.; Thingna, J.; Cao, J.; Lim, C. T. Single molecule and multiple bond characterization of catch bond associated cytoadhesion in malaria. *Sci. Rep.* **2017**, *7* (1), 4208.
(32) Cooke, B. M.; Berendt, A. R.; Craig, A. G.; MacGregor, J.; Newbold, C. I.; Nash, G. B. Rolling and stationary cytoadhesion of red blood cells parasitized by *Plasmodium falciparum*: separate roles for ICAM-1, CD36 and thrombospondin. *Br. J. Hamaetol.* **1994**, *87* (1), 162−170.
(33) McCormick, C. J.; Craig, A.; Roberts, D.; Newbold, C. I.; Berendt, A. R. Intercellular adhesion molecule-1 and CD36 synergize to mediate adherence of *Plasmodium falciparum*-infected erythrocytes to cultured human microvascular endothelial cells. *J. Clin. Invest.* **1997**, *100* (10), 2521−2529.
(34) Herricks, T.; Seydel, K. B.; Turner, G.; Molyneux, M.; Heyderman, R.; Taylor, T.; Rathod, P. K. A microfluidic system to study cytoadhesion of *Plasmodium falciparum* infected erythrocytes to primary brain microvascularendothelial cells. *Lab Chip* **2011**, *11* (17), 2994−3000.
(35) Qiu, Y.; Ahn, B.; Sakurai, Y.; Hansen, C. E.; Tran, R.; Mimche, P. N.; Mannino, R. G.; Ciciliano, J. C.; Lamb, T. J.; Joiner, C. H.; Ofori-Acquah, S. F.; Lam, W. A. Microvasculature-on-a-chip for the long-term study of endothelial barrier dysfunction and microvascular obstruction in disease. *Nat. Biomed. Eng.* **2018**, *2*, 453−463.
(36) Tanaka, M.; Lanzer, M. Receptor-functionalized lipid membranes as biomimetic surfaces for adhesion of *Plasmodium falciparum*-infected erythrocytes. *Methods Mol. Biol.* **2022**, *2470*, 601−613.
(37) Fröhlich, B.; Dasanna, A. K.; Lansche, C.; Czajor, J.; Sanchez, C. P.; Cyrklaff, M.; Yamamoto, A.; Craig, A.; Schwarz, U. S.; Lanzer, M.; Tanaka, M. Functionalized supported membranes for quantifying adhesion of *P. falciparum*-infected erythrocytes. *Biophys. J.* **2021**, *120* (16), 3315−3328.
(38) Rieger, H.; Yoshikawa, H. Y.; Quadt, K.; Nielsen, M. A.; Sanchez, C. P.; Salanti, A.; Tanaka, M.; Lanzer, M. Cytoadhesion of *Plasmodium falciparum*-infected erythrocytes to chondroitin-4-sulfate is cooperative and shear enhanced. *Blood* **2015**, *125* (2), 383−391.
(39) Bachmann, A.; Metwally, N. G.; Allweier, J.; Cronshagen, J.; Del Pilar Martinez Tauler, M.; Murk, A.; Roth, L. K.; Torabi, H.; Wu, Y.; Gutsmann, T.; Bruchhaus, I. CD36 - A host receptor necessary for malaria parasites to establish and maintain infection. *Microorganisms* **2022**, *10* (12), 2356.

https://doi.org/10.1021/acsinfecdis.5c00594
ACS Infect. Dis. XXXX, XXX, XXX−XXX

(40) Nourshargh, S.; Alon, R. Leukocyte migration into inflamed tissues. *Immunity* **2014**, *41* (5), 694−707.
(41) Korn, C. B.; Schwarz, U. S. Dynamic states of cells adhering in shear flow: From slipping to rolling. *Phys. Rev. E* **2008**, *77* (4), 041904.
(42) Dasanna, A. K.; Lansche, C.; Lanzer, M.; Schwarz, U. S. Rolling adhesion of schizont stage malaria-infected red blood cells in shear flow. *Biophys. J.* **2017**, *112* (9), 1908−1919.
(43) Li, I. T.; Ha, T.; Chemla, Y. R. Mapping cell surface adhesion by rotation tracking and adhesion footprinting. *Sci. Rep.* **2017**, *7*, 44502.
(44) Kim, K.; Saleh, O. A. Stabilizing method for reflection interference contrast microscopy. *Appl. Opt.* **2008**, *47* (12), 2070−2075.
(45) Wang, X.; Ha, T. Defining single molecular forces required to activate integrin and notch signaling. *Science* **2013**, *340* (6135), 991−994.
(46) de Gennes, P.-G. Maximum pull out force on DNA hybrids. *C. R. Acad. Sci., Ser. IV:Phys.* **2001**, *2* (10), 1505−1508.
(47) Turgeon, M. L. *Clinical Hematology: Theory and Procedures* 5th ed.; Lippincott Williams & Wilkins, 2011.
(48) Sanchez, C. P.; Karathanasis, C.; Sanchez, R.; Cyrklaff, M.; Jäger, J.; Buchholz, B.; Schwarz, U. S.; Heilemann, M.; Lanzer, M. Single-molecule imaging and quantification of the immune-variant adhesin VAR2CSA on knobs of *Plasmodium falciparum*-infected erythrocytes. *Commun. Biol.* **2019**, *2*, 172.
(49) Fedosov, D. A.; Caswell, B.; Karniadakis, G. E. A multiscale red blood cell model with accurate mechanics, rheology, and dynamics. *Biophys. J.* **2010**, *98* (10), 2215−2225.
(50) Fedosov, D. A.; Noguchi, H.; Gompper, G. Multiscale modeling of blood flow: from single cells to blood rheology. *Biomech. Model. Mechanobiol.* **2014**, *13* (2), 239−258.
(51) Evans, E. A.; Calderwood, D. A. Forces and bond dynamics in cell adhesion. *Science* **2007**, *316* (5828), 1148−1153.
(52) Lubiana, P.; Bouws, P.; Roth, L. K.; Dörpinghaus, M.; Rehn, T.; Brehmer, J.; Wichers, J. S.; Bachmann, A.; Höhn, K.; Roeder, T.; Thye, T.; Gutsmann, T.; Burmester, T.; Bruchhaus, I.; Metwally, N. G. Adhesion between *P. falciparum* infected erythrocytes and human endothelial receptors follows alternative binding dynamics under flow and febrile conditions. *Sci. Rep.* **2020**, *10* (1), 4548.
(53) Ishida, S.; Ami, A.; Imai, Y. Factors diminishing cytoadhesion of red blood cells infected by *Plasmodium falciparum* in arterioles. *Biophys. J.* **2017**, *113* (5), 1163−1172.
(54) Rowe, J. A.; Handel, I. G.; Thera, M. A.; Deans, A. M.; Lyke, K. E.; Koné, A.; Diallo, D. A.; Raza, A.; Kai, O.; Marsh, K.; Plowe, C. V.; Doumbo, O. K.; Moulds, J. M. Blood group O protects against severe *Plasmodium falciparum* malaria through the mechanism of reduced rosetting. *Proc. Natl. Acad. Sci. U.S A.* **2007**, *104* (44), 17471−17476.
(55) Chamberlain, S. G.; Iwanaga, S.; Higgins, M. K. Immune evasion runs in the family: two surface protein families of *Plasmodium falciparum*-infected erythrocytes. *Curr. Opin. Microbiol.* **2025**, *85*, 102598.
(56) Albrecht, C.; Blank, K.; Lalic-Mülthaler, M.; Hirler, S.; Mai, T.; Gilbert, I.; Schiffmann, S.; Bayer, T.; Clausen-Schaumann, H.; Gaub, H. E. DNA: A programmable force sensor. *Science* **2003**, *301* (5631), 367−370.
(57) Yasunaga, A. B.; Li, I. T. S. Quantification of fast molecular adhesion by fluorescence footprinting. *Sci. Adv.* **2021**, *7* (34), No. eabe6984.
(58) Liu, Y.; Blanchfield, L.; Ma, V. P.-Y.; Andargachew, R.; Galior, K.; Liu, Z.; Evavold, B.; Salaita, K. DNA-based nanoparticle tension sensors reveal that T-cell receptors transmit defined pN forces to their antigens for enhanced fidelity. *Proc. Natl. Acad. Sci. U.S A.* **2016**, *113* (20), 5610−5615.
(59) Wang, X.; Rahil, Z.; Li, I. T. S.; Chowdhury, F.; Leckband, D. E.; Chemla, Y. R.; Ha, T. Constructing modular and universal single molecule tension sensor using protein G to study mechano-sensitive receptors. *Sci. Rep.* **2016**, *6* (1), 21584.
(60) Pennarola, F.; Cavalcanti-Adam, E. A. Surface patterning for the control of receptor clustering and molecular forces of integrin-mediated adhesions. *Methods Mol. Biol.* **2021**, *2217*, 183−195.
(61) Dupire, J.; Socol, M.; Viallat, A. Full dynamics of a red blood cell in shear flow. *Proc. Natl. Acad. Sci. U.S A.* **2012**, *109* (51), 20808−20813.
(62) Félétou, M. Colloquium Series on Integrated Systems Physiology: from Molecule to Function to Disease. In *The Endothelium: Part 1: Multiple Functions of the Endothelial Cells−Focus on Endothelium-Derived Vasoactive Mediators*; Morgan & Claypool Life Sciences, 2011.
(63) Lambros, C.; Vanderberg, J. P. Synchronization of *Plasmodium falciparum* erythrocytic stages in culture. *J. Parasitol.* **1979**, *65* (3), 418−420.
(64) Staalsoe, T.; Giha, H. A.; Dodoo, D.; Theander, T. G.; Hviid, L. Detection of antibodies to variant antigens on *Plasmodium falciparum*-infected erythrocytes by flow cytometry. *Cytometry* **1999**, *35* (4), 329−336.
(65) Kaindl, T.; Rieger, H.; Kaschel, L. M.; Engel, U.; Schmaus, A.; Sleeman, J.; Tanaka, M. Spatio-temporal patterns of pancreatic cancer cells expressing CD44 isoforms on supported membranes displaying hyaluronic acid oligomers arrays. *PLoS One* **2012**, *7* (8), No. e42991.
(66) Ohta, T.; Monzel, C.; Becker, A. S.; Ho, A. D.; Tanaka, M. Simple physical model unravels influences of chemokine on shape deformation and migration of human hematopoietic stem cells. *Sci. Rep.* **2018**, *8* (1), 10630.
(67) Gompper, G.; Ihle, T.; Kroll, D. M.; Winkler, R. G. Multi-Particle Collision Dynamics: A Particle-Based Mesoscale Simulation Approach to the Hydrodynamics of Complex Fluids. In *Advanced Computer Simulation Approaches for Soft Matter Sciences III*; Holm, C., Kremer, K., Eds.; Springer Berlin Heidelberg, 2009; pp 1−87.
(68) Malevanets, A.; Kapral, R. Mesoscopic model for solvent dynamics. *J. Chem. Phys.* **1999**, *110* (17), 8605−8613.
(69) Dasanna, A. K.; Fedosov, D. A.; Gompper, G.; Schwarz, U. S. State diagram for wall adhesion of red blood cells in shear flow: from crawling to flipping. *Soft Matter* **2019**, *15* (27), 5511−5520.
(70) Bell, G. I. Models for the specific adhesion of cells to cells. *Science* **1978**, *200* (4342), 618−627.
(71) Virtanen, P.; Gommers, R.; Oliphant, T. E.; Haberland, M.; Reddy, T.; Cournapeau, D.; Burovski, E.; Peterson, P.; Weckesser, W.; Bright, J.; van der Walt, S. J.; Brett, M.; Wilson, J.; Millman, K. J.; Mayorov, N.; Nelson, A. R. J.; Jones, E.; Kern, R.; Larson, E.; Carey, C. J.; Polat, İ.; Feng, Y.; Moore, E. W.; VanderPlas, J.; Laxalde, D.; Perktold, J.; Cimrman, R.; Henriksen, I.; Quintero, E. A.; Harris, C. R.; Archibald, A. M.; Ribeiro, A. H.; Pedregosa, F.; van Mulbregt, P.; et al. SciPy 1.0: Fundamental algorithms for scientific computing in Python. *Nat. Methods* **2020**, *17* (3), 261−272.
(72) Quadt, K. A.; Barfod, L.; Andersen, D.; Bruun, J.; Gyan, B.; Hassenkam, T.; Ofori, M. F.; Hviid, L. The density of knobs on *Plasmodium falciparum*-infected erythrocytes depends on developmental age and varies among isolates. *PLoS One* **2012**, *7* (9), No. e45658.

https://doi.org/10.1021/acsinfecdis.5c00594
ACS Infect. Dis. XXXX, XXX, XXX−XXX